ELSEVIER

Polymer 42 (2001) 199–208

polymer

www.elsevier.nl/locate/polymer

Effect of micromorphologic features on the interfacial strength of iPP/Kevlar fiber microcomposites ☆

Chang-Mou Wu[a,1], Ming Chen[a,*], J. Karger-Kocsis[b]

[a]*Institute of Materials Science and Engineering, National Sun Yat-Sen University, Kaohsiung 80424, Taiwan, ROC*
[b]*Institut für Verbundwerkstoffe GmbH, Universität Kaiserslautern, Pf. 3049, Kaiserslautern D-67653, Germany*

Received 4 January 2000; received in revised form 10 April 2000; accepted 14 April 2000

Abstract

Fully transcrystalline, fully spherulitic specimens, and single Kevlar fiber microcomposites were prepared for isotactic polypropylene (iPP) resin with positive, negative, or mixed birefringence and annealed condition. The micromorphologic observation (PLM, PCLM, SEM, AFM) and supermolecular structure study (WAXS, SAXS) show that the optical birefringence change of iPP is related to the contribution of cross-hatch lamellae. Transcrystalline layers along a Kevlar fiber were about 50 μm thick. The interfacial shear strength was determined by means of a modified single fiber pull-out test. The more radial lamellae increase the radial stiffness relative to the tangential one, and produce higher normal stresses on the fiber surface. The results revealed that the optical birefringence in the transcrystalline layer significantly affected the interfacial shear strength, which was related to the mechanical friction, thermal mismatch, and the crystallinity. © 2000 Elsevier Science Ltd. All rights reserved.

Keywords: Polypropylene; Transcrystalline; Pull-out

1. Introduction

The interface between reinforcing fibers and the matrix in composite materials is widely regarded as an important factor determining the mechanical property profile. Especially when the processing of semicrystalline thermoplastic materials is considered, changes in the matrix morphology around the fibers must be taken into account. These microstructural changes may affect the fiber/matrix adhesion and can thus be treated as additional interphase parameters. It is not yet clear how different morphological structures induced by the processing of thermoplastic composites are really essential with respect to the interfacial shear strength and the related failure. From the surveyed literature, transcrystalline superstructures developed around the reinforcing fibers are reported either to promote interfacial shear strength of isotactic polypropylene (iPP) composites [1–3] or to have no influence [4–8] at all. Several authors have emphasized the effects of thermal shrinkage stresses acting perpendicular to the fiber surface, which in turn increased the interfacial friction [9–11]. Besides these, the influences of crystallinity [6,7], thickness of the transcrystalline layer [2], wetting and de-wetting [6], have also been discussed.

The influence of the transcrystalline layer on the properties has been studied, but the properties of the transcrystalline layer itself have been less investigated. One of the reasons is the inability in most cases to isolate the contribution of the transcrystalline layer from the crystalline matrix. Early reports showed that the strain to failure in a transcrystalline layer of PP is only 4% versus 300% for a spherulitic sample [12]. Hata et al. [13] investigated the mechanical properties of transcrystalline layers. They prepared an all-transcrystalline film of PP with more than 300 μm thickness between two sheets of polytetrafluoroethylene (PTFE). The transcrystalline film could be stretched up to 800% accompanied by the development of opacity and necking. This is a very unusual for crystalline materials with very high degrees of crystallization and orientation. However, the spherulite film could be stretched up to 30% at maximum, exhibiting brittle fracture. Recently, the transcrystallization behavior of Nylon 66 in the presence of Aramid fiber reinforcement was investigated by a dynamic mechanical thermal analyzer [14]. The strips of all-transcrystalline specimens were cut from the microcomposite samples using a microtome. For

☆ Presented at the symposium of The First Asian–Australasian Conference on Composite Materials (ACCM-1) in Osaka, Japan, 7–9 October 1998.

* Corresponding author. Tel.: +886-7-5252000-4062; fax: +886-7-525-4099.

E-mail address: mingchen@mail.nsysu.edu.tw (M. Chen).

[1] Current address: Institute of Chemistry, Academia Sinica, Taipei, Taiwan 115, ROC.

0032-3861/01/$ - see front matter © 2000 Elsevier Science Ltd. All rights reserved.
PII: S0032-3861(00)00312-8

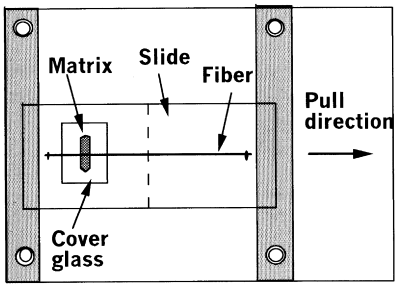

Fig. 1. Schematic drawing of the specimen and the set-up used for the modified single-fiber pull-out test.

the transcrystalline layer, the damping energy was half reduced, and the dynamic modulus was double when compared to the respective properties of the crystallized matrix. Zeng et al. [15] found the Young's modulus of the transcrystalline zone was higher than that of bulk spherulites, i.e. the stiffness of the material with transcrystalline zone was improved. It was suggested that the transcrystalline layer could reduce the thermal mismatch of the constituents, and thereby decrease the thermal stresses due to the alignment of its crystallites.

The formation of spherulites with positive and mixed optical character is unexpected in polymers. As reviewed by Norton and Keller [16], there exist three spherulite types of α-iPP with different optical birefringence as determined by the nature of the lamellae and their mutual arrangement. Spherulites of α-iPP are composed of a mainframe of dominant lamellae radiating from the spherulitic center and infilling tangential (or, "cross-hatched") lamellae in the interstitial regions. This formation of the cross-hatched lamellae has been attributed [17,18] to crystallographic branching at an angle of ca. 80° via twinning. Since the degree of the branching is temperature-dependent, this leads to birefringence changes in spherulites crystallized at different temperatures. From the above review, transcrystalline interphase has been shown to have significantly different properties compared to the bulk matrix. The unique properties of transcrystalline layer have been rarely studied because the isolation of the transcrystalline layer from the crystalline matrix is still a challenging task.

In a preceding study [19], the transcrystalline effect on the interfacial shear strength in a single carbon fiber (CF) reinforced syndiotactic polypropylene (sPP) and iPP composites was evaluated by single fiber fragmentation. The flat-on lamellae along with a high amorphous fraction in the transcrystalline interphase of sPP/CF were suggested to be responsible for improved interfacial shear strength. However, a poor interfacial adhesion existed between iPP and high-modulus CF even in the presence of transcrystallinity, because the orientation of lamellae was edge-on. As we are gradually understanding the formation and crystallization behavior of the transcrystalline layer in iPP resin [20], specific micromorphologic structure of the iPP resin with positive, negative, or mixed birefringence and annealed specimens can therefore be prepared.

In this study, micromorphologic features and supermolecular structure of all transcrystalline and all spherulitic iPP were investigated through polarized light microscopy (PLM), phase contrast optical microscopy (PCLM), scanning electron microscopy (SEM), atomic force microscopy (AFM), wide-angle X-ray scattering (WAXS), and small-angle X-ray scattering (SAXS). Attention has been focused on the changes of optical textures of the transcrystalline interphase by a series of thermal events in single fiber thermoplastic composites. Transcrystalline layers of various build-up birefringence but with similar thickness were produced along a Kevlar fiber. A modified single fiber pull-out test was used to determine the interfacial shear strength and failure mechanisms under observation by PLM.

Table 1
Crystallization conditions and birefringence of iPP specimens which were first kept at 200°C for 5 min in order to melt the crystal residues

Birefringence	Crystallization conditions
Mixed	Crystallized at 133°C for 1 h
Positive	Crystallized at 133°C for 1 h, then heated to 169°C and cooled to 30°C at 10°C/min
Annealed	Crystallized at 133°C for 1 h, then heated to 160°C and annealed for 8 h
Negative	Crystallized at 141°C for 6 h

2. Experimental

2.1. Materials, specimens preparation and pull-out test

The iPP film utilized in this study was Novolen, 1100N grade, marketed by BASF (Germany). Its glass transition and equilibrium melting temperatures were 0 and 185°C, respectively. An Aramid fiber (Kevlar 49, DuPont, USA) was used in this study for the pull-out test. A specimen with about 500 μm embedded fiber length was prepared as follows. A single fiber was fixed at both ends by an adhensive and then sandwiched between two iPP strips, which were then melt compressed between two cover glasses. Pull-out tests were performed in a specially designed and home-made micro-tensile testing machine. This device allowed us to monitor the pull-out process by a transmitted light microscope [5]. Fig. 1 illustrates the specimen and the set-up used for the modified single-fiber pull-out test. The broken line indicates that the slides were cut into two separate pieces before the pull-out test. Detailed thermal and annealing conditions are given in Table 1. By using the above procedures, four types of specimens were made with different birefringence. It should be remembered that in these specimens the transcrystallization has been produced under quiescent conditions. Single-fiber pull-out tests were conducted at room temperature with a constant cross-head speed of 0.5 mm/min. Since iPP is a ductile

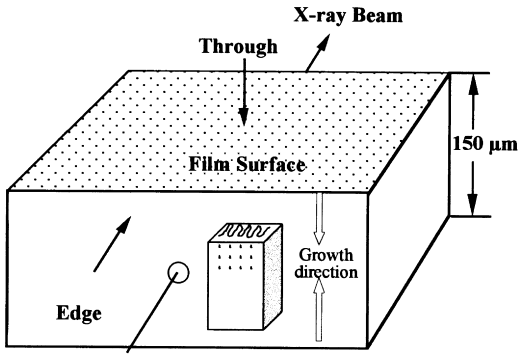

Fig. 2. Schematic drawing of the X-ray beam direction in the WAXS and SAXS experiments for all transcrystalline iPP specimen.

material, uniform shear yielding of the interface is assumed at least at the specimen thickness set (ca. 50 μm). The interfacial shear strength, τ_i, can be calculated from Eq. (1)

$$\tau_i = \frac{F_{max}}{\pi DL} \quad (1)$$

where F_{max} is the maximum tensile load, and D and L are the fiber diameter and the embedded fiber length, respectively.

2.2. Micromorphologic observation

Single fiber specimens were prepared in a hot stage of a Leitz Dialux 20 microscope. The specimens were heated to 200°C and maintained at this molten state for 5 min. The hot stage was then cooled to the crystallization temperature ($T_c = 133$ or 141°C) at a rate of 40°C/min. Crystallizing the iPP/single fiber specimen isothermally at $T_c = 133$°C for 1 h resulted in a mixed mode morphology, whereas crystallizing the specimen at $T_c = 141$°C for 6 h led to a negative birefringence structure. Two more thermal conditions used to prepare specimens with different birefringence are compared in Table 1. The optical character, i.e. the sign of birefringence of the micromorphologic feature was determined by means of a primary red filter (λ-plate) located diagonally between cross polarizers. These specimens were later etched chemically according to the procedure of Olley and Bassett [21] in order to study the micromorphological changes in different specimens by PCLM (Leitz, Wetzlar, Germany), AFM, and SEM (JEOL 6400). AFM experiments were performed at ambient condition in a tapping mode by using a NanoScope IIIa setup (Digital Instruments). Detailed equipment setup was published in a previous publication [20].

2.3. Supermolecular structure

The crystal structure of fully transcrystalline and fully spherulitic specimens was separately estimated by using both WAXS and SAXS. For fully transcrystalline specimens [13,22], the iPP film was sandwiched between two PTFE sheets. Each sample of diameter 6 mm was punched from the sandwich and sealed in a DSC (Differential Scanning Calorimeter) aluminum pan for further thermal treatment in a Perkin–Elmer DSC-7. The thermal and annealing conditions were the same as described in the previous section and in Table 1. Fully transcrystalline specimens were ready for X-ray diffraction studies by removing the iPP specimens from the DSC pans and the PTFE sheets. The fully spherulitic specimens were prepared in the same procedures without using PTFE sheets.

The WAXS/SAXS instrument (Material Analysis and Characterization Science Co., Japan) was assembled with a maximum camera length of 200 cm and Nickel-filtered CuK_α radiation of 45 KV × 200 mA with a characteristic wavelength of 0.1542 nm. The camera length for WAXS

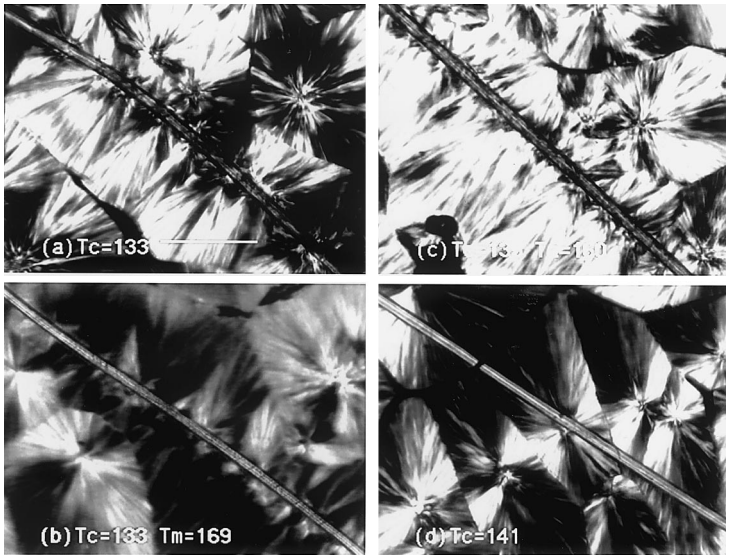

Fig. 3. PLM micrographs of the transcrystallized regions and the spherulites with different birefringence: (a) mixed; (b) positive; (c) annealed; and (d) negative. The scale bar corresponds to 50 μm.

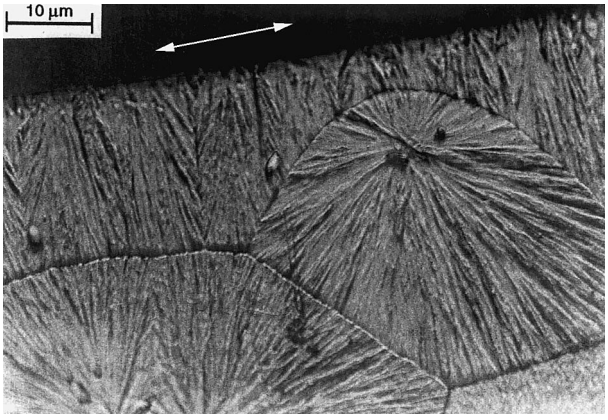

Fig. 4. PCLM micrograph showing the micromorphology of etched iPP specimen with mixed birefringence. The scale bar corresponds to 10 μm. (Note: arrow indicates the position of fiber removed during etching.)

and SAXS were 60 and 200 cm, respectively. Fig. 2 shows the beam direction in the WAXS and SAXS experiments for all transcrystalline iPP. Specimens with thickness of 150 μm were penetrated by a X-ray beam in through and edge views. No correction was applied to the WAXS and SAXS diffraction for all the fully spherulitic and transcrystalline specimens. The azimuthal scanning results was read and analyzed by an ImageQuant® software.

2.4. Crystallinity determination and thermal expansion determination

The degree of crystallinity of fully transcrystalline and fully spherulitic specimens was separately estimated by using both DSC and X-ray diffraction methods. The melting behavior and the heat fusion were studied using the Perkin–Elmer DSC-7. Both temperature and heat flow scale were calibrated with indium at a heating rate of 20°C/min under a constant nitrogen flux. The degree of crystallinity was calculated by reference to the melting enthalpy of the 100% crystalline iPP, 207.1 J/g [23,24]. The WAXS instrument used here was Diano 8536 with Nickel-filtered CuK_α radiation and a characteristic wavelength of 0.1542 nm. The area of main crystalline peaks, which were subtracted by a scaled background curve, divided by the total area was taken as the X-ray crystallinity.

Thermal expansion measurements were performed in a Mettler thermomechanical analyzer (TMA 40). Fully spherulitic specimens were heated from 30 to 130°C at a rate of 5°C/min and tested under a compression load of 0.05 N. The linear slope between 40 and 80°C in the second run was used as the thermal expansion coefficient.

3. Results and discussion

3.1. Morphological observation

Fig. 3a–d show the PLM micrographs of single Kevlar fiber/iPP microcomposites prepared for the pull-out test under four different thermal conditions, as described in the second column of Table 1. A well-defined transcrystalline layer with about 50 μm thickness is observed in Fig. 3a–c. In Fig. 3a, the mixed birefringence is clearly seen by inspecting the lighter and darker strips alternate irregularly. In the second thermal condition, the specimen described above was heated to 169°C and immediately recrystallized at a cooling rate of 10°C/min, whereupon the mixed birefringence was transformed into a positive one and the boundary of the spherulites became obscure (see Fig. 3b).

The specimen with mixed birefringence was heated to 160°C at a rate of 10°C/min and annealed for 8 h, as described in the third condition of Table 1. Negative birefringence was clearly observed after the melting of crosshatch lamellae when heating the specimen to 160°C initially. After being annealed for 8 h, the color changed slightly due to the lamellae thickening. The annealed specimen shows a tendency of (weak) negative birefringence with a well-resolved Maltese cross pattern (see Fig. 3c). The colors in the different quadrants are not easy to identify in Fig. 3c, because of lamellae thickness and the morphology colored even without a gypsum plate. The first step of the second and the third thermal conditions of Table 1 induced the same birefringence and had the similar thickness of the transcrystalline layer along the fiber as did the first thermal condition. The thickness of the transcrystalline layer also had the order of the spherulite radius.

Negative birefringence (blue appears in quadrants II and IV and yellow in quadrants I and III) is clearly observed in Fig. 3d for a specimen isothermally crystallized at 141°C for 6 h. It can be seen that no transcrystalline layer is induced around the fiber, and the spherulites show a well-resolved Maltese cross pattern. Crystallization at 141°C is above the boundary temperature (139°C) for transcrystallization under quiescent conditions. It has been shown that the formation of a transcrystalline layer in melt-crystallized iPP is very sensitive to the temperature. A change of 8°C in the temperature of crystallization resulted in a change from a transcrystalline morphology to a fully spherulitic morphology (cf. Fig. 3a and d).

Under the assumptions of uniaxial crystal and three orthogonal axes, the birefringence of α-iPP spherulites (Δ_s) can be written as [25,26]:

$$\Delta_s = \left(\frac{3t-1}{2}\right)(n_c - n_a) = \left(t - \frac{r}{2}\right)(n_c - n_a) \qquad (2)$$

where r and t are the fractions of radial and tangential lamellae ($r + t = 1$), and n_c and n_a are the refractive indices parallel to the *c*- and *a*-axes, respectively. The relative amounts of radial and tangential lamellae can be estimated from the sign of birefringence. This equation explains why α-spherulites exhibit positive birefringence when the fraction of tangential lamellae is larger than 1/3($t > 1/3$). For the specimen crystallized at $T_c = 141$°C for 6 h, negative birefringence indicated that $0 < t < 1/3$. The fraction of

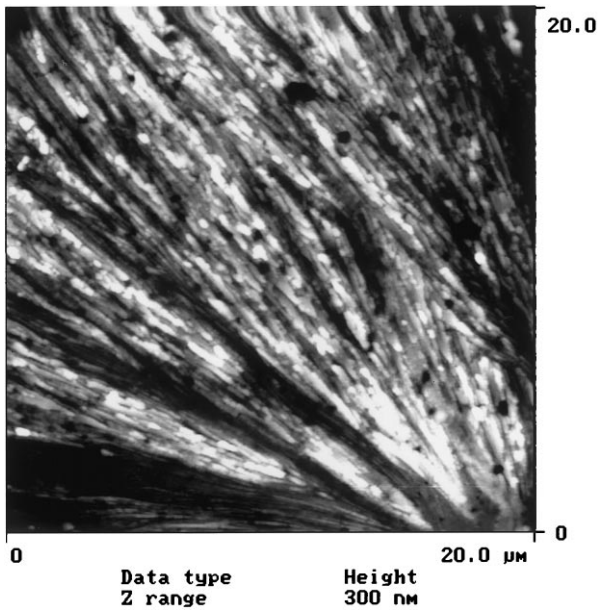

Fig. 5. AFM height image showing the micromorphology of etched iPP specimen with mixed birefringence: radial lamellae and 'nodular' textures. Image size: 20 μm × 20 μm.

tangential lamellae is around 1/3 for specimens with mixed birefringence (crystallized at $T_c = 133$°C for 1 h).

3.2. Characterization of micromorphologic features

Fig. 4 shows the micromorphologic feature of the etched transcrystalline and spherulitic layer in iPP microcomposites with mixed birefringence obtained by PCLM. The lamellae lay-up in the transcrystalline region seems to be very similar what was observed in spherulites of the bulk. As displayed in the AFM image of Fig. 5, the etched specimen with mixed birefringence shows the radial lamellae and 'nodular' textures which are thought to represent the earliest stages of branching [16]. The dominant lamellae grow regularly and the nodular textures seem to be mostly present in lateral regions. Fig. 6 shows the AFM image of a specimen with positive birefringence, radial lamellae coexist with sufficient amount of cross-hatched (or tangential) lamellae [18,27]. The change in birefringence of iPP can be explained in terms of contributions from the two lamellae components, radial and tangential [28].

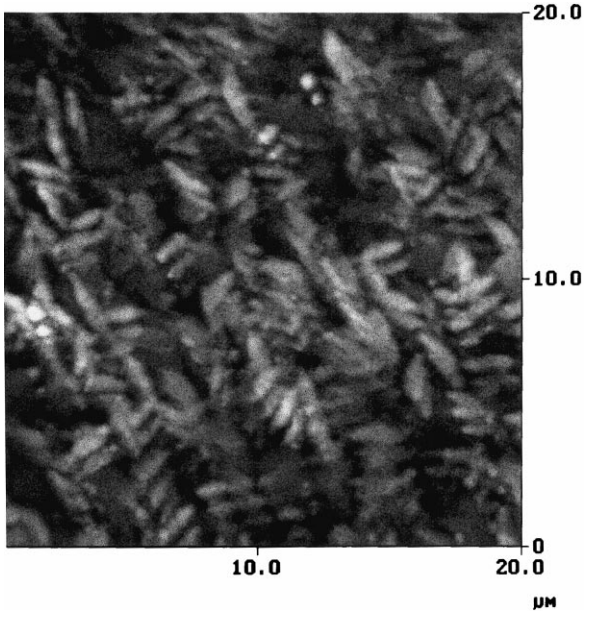

Fig. 6. Tapping AFM image of the etched iPP specimen with positive birefringence. Radial lamellae and cross-hatch lamellae are clear displayed. Image size: 20 μm × 20 μm.

The micromorphologic features in the specimen annealed at 160°C seem to be very similar to what was observed in the mixed birefringence specimen. A clear radial and cross-hatch lamellae arrangement taken by the SEM is displayed in Fig. 7. The SEM micrograph shown in Fig. 8 depicts radial lamellae and some 'nodular' textures. It suggests that a small amount of the cross-hatch lamellae still exists in the negative birefringence specimen. The results are consistent with the study [18] which concluded that cross-hatch lamellae vanished only from crystallization above 155°C.

3.3. Characterization of supermolecular structures

Fig. 9 shows the WAXS patterns taken from four different thermal conditions and two perpendicular view directions. An isotropic Debye ring pattern is observed in the through view of all spherulitic and all transcrystalline specimens. More diffuse ring patterns without orientation are observed in the positive birefringence specimen. It suggests that the positive birefringence specimen presents less ordering in the view direction. A clear oriented diffraction pattern from the edge view with the same reflections is observed in mixed, negative birefringence and annealed specimens.

The degree of orientation (degree of parallelity) [29], calculated from the azimuthal scans of the (110), (040) and (130) reflections, are listed in Table 2 for the edge view transcrystalline specimens with different birefringence. Positive birefringence specimen exhibits zero degree of orientation as displayed in the WAXS pattern. This may be due to the compensated contribution of radial and cross-hatch lamellae under these detected directions. From the orientation degree obtained from the (110) and (130) reflections, the mixed birefringence specimen gives better orientation (relative increment of 1.2···2.4%, cf. Table 2). Whereas, negative birefringence and annealed specimens exhibit the same orientation degree for the (110) and (130) reflections. In the (040) reflection, the negative birefringence specimen exhibits 86.11% degree of orientation, which is better than that of mixed birefringence specimen of 83.89% and the annealed specimen of 83.39%. Since the (040) reflection is composed of contributions from both the radial and cross-hatch lamellae, the cross-hatch lamellae might affect the degree of orientation. However, it seems

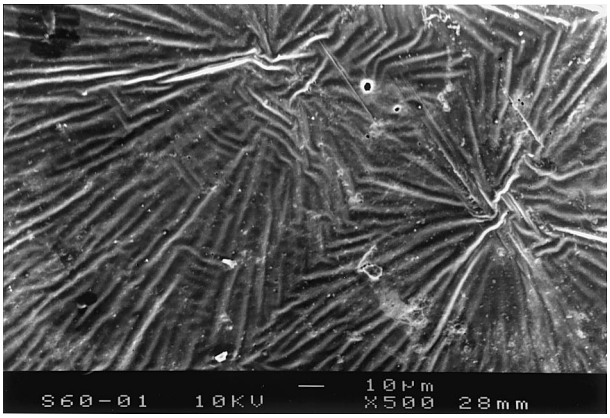

Fig. 7. SEM micrograph showing the micromorphology of etched iPP specimen after annealed at 160°C. Radial lamellae and cross-hatch lamellae can be found clearly. The scale bar corresponds to 10 μm.

that there is no much difference in the degree of orientation in these three specimens.

Fig. 10 shows the SAXS patterns taken from four different thermal conditions and two perpendicular view directions. Fig. 11 shows the SAXS intensity as a function of Q for all spherulitic and transcrystalline specimens with annealed condition. The long period of all transcrystalline iPP can be determined from the peak Q value of the shoulder, and the results are listed in the fourth column of Table 3. The corresponding long-periods were 26, 22, 33 and 30 nm, respectively, for specimens with mixed, positive, annealed, and negative birefringence iPP. The long-period obtained by edge and through view exhibits the same value, and the long-period in the all transcrystalline and all spherulitic specimens do not produce significant difference as well.

3.4. Degree of crystallinity, melting behavior and thermal expansion

Fig. 12 shows the DSC heating scans at a rate of 20°C/min for all transcrystalline iPP specimens with different birefrin-

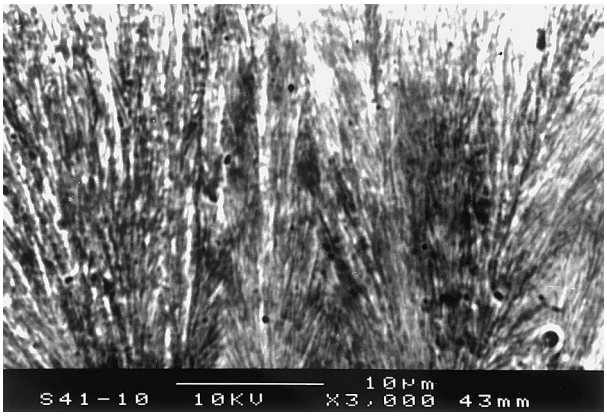

Fig. 8. SEM micrograph showing the micromorphology of etched iPP specimen with negative birefringence. The scale bar corresponds to 10 μm.

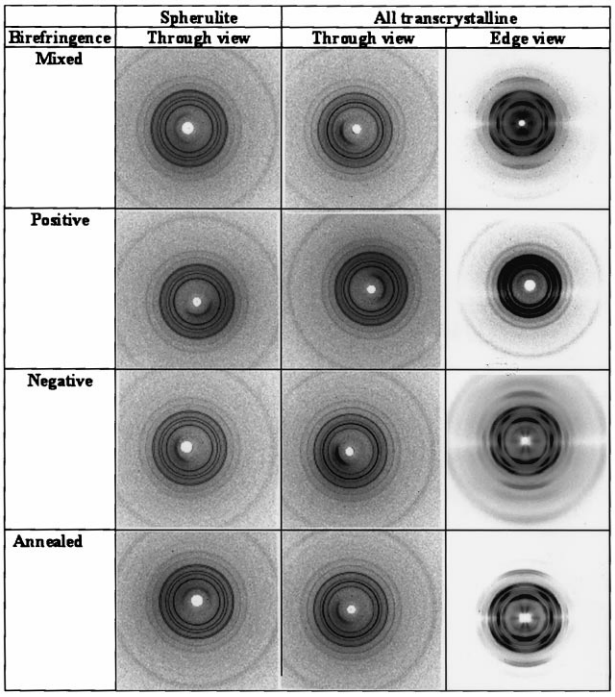

Fig. 9. WAXS patterns taken from two perpendicular beam directions for all spherulitic and all transcrystalline iPP specimens with different optical birefringence.

gence. From the literature and the DSC melting traces, the melting peaks were strongly dependent on the thermal history of iPP. The occurrence of double-melting peaks is a common feature for semicrystalline polymers crystallized isothermally. Specimen with mixed birefringence which was crystallized at 133°C (regime III) for 1 h shows a broad, smaller, low-melting peak at 158.0°C (α_1, T_m^1) and a larger melting peak at 168.8°C (α_2, T_m^2). An interpretation has been attributed to a recrystallization of the α_1 form into α_2 form and this recrystallization process between two α-modifications having different crystal order (α_1 and α_2) [23]. Specimen crystallized at 141°C (regime II) for 6 h has a lower α_1-crystalline melting peak at 163.8°C and a larger α_2-crystalline melting peak at 174.6°C. The low-melting peak temperatures (T_m^1) of both specimens are 23–25°C above the crystallization temperature because the crystallization time is much longer than the required time for crystallization completion.

Table 2
Degree of orientation of all transcrystalline iPP specimens with different birefringence

Birefringence	Degree of orientation (%)		
	(110)	(040)	(130)
Mixed	64.92	83.89	87.22
Positive	0	0	0
Annealed	63.28	83.39	86.06
Negative	62.50	86.11	86.06

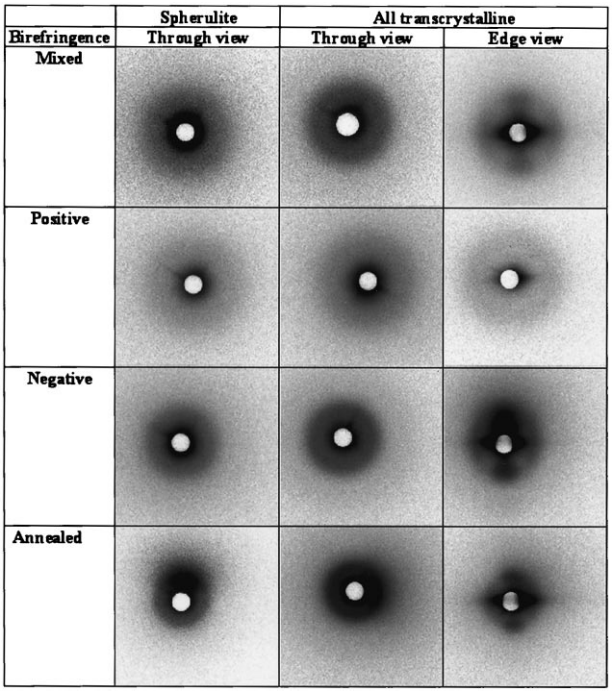

Fig. 10. SAXS patterns taken from two perpendicular beam directions for all spherulitic and transcrystalline iPP specimens with different optical birefringence.

The area underneath the melting peaks was integrated and the crystallinity was calculated by dividing by the heat of fusion by 207.1 J/g [23,24]. The crystallinities measured by the DSC method are listed in the second column of Table 3. The values were 54 and 59%, respectively, for mixed and negative birefringence iPP. Specimens annealed at 160°C for 8 h presented a single crystalline melting peak at 173.5°C which shows a decrease of 1.1°C in T_m^2, compared with the negative ones. The corresponding crystallinity obtained by DSC is also 6 wt% lower. The phenomenon of lower crystallinity, lower melting temperature for specimens annealed at higher temperature (160°C) is an unexpected result. It indicated the melting-recrystallization was not significant in the third thermal condition in which iPP specimens were annealed in regime II. The characteristic low-melting peak (α_1) may be merged with the high-melting peak (α_2) to form a single melting peak with a little lower melting temperature in the annealed specimens. Specimens with positive birefringence show the typical melting behavior of nonisothermal crystallization, a broad, single melting peak at 164.3°C. In this crystallization condition, mixed birefringence iPP was first heated to 169°C, which was above the high-melting peak (168.8°C) of mixed birefringence iPP, and most of crystals were melted before melt crystallization. Positive birefringence iPP specimens have the lowest degree of crystallinity, 53%.

The degree of crystallinity obtained by WAXS for all transcrystalline iPP specimens is listed in the third column of Table 3. The crystallinities were 46, 38, 52 and 50%, respectively, for specimens with mixed, positive, annealed and negative birefringence iPP. As listed in the fourth column of Table 3, the corresponding long-periods were 26, 22, 33 and 30 nm, respectively, which is consistent with the crystallinity trends obtained by WAXS. The specimen annealed at 160°C for 8 h showed an increase of 3 nm (10%) in the long-period, and an increase of 2% in the crystallinity, compared with the specimen isothermally crystallized at 141°C for 6 h. Higher crystallization temperature produced structurally more perfect transcrystalline layers or spherulites and increased the degree of crystallinity. The apparent crystallinity obtained by DSC method were 8, 15, 1 and 9% higher than the corresponding crystallinity determined by WAXS. The apparent crystallinities of double-melting peaks were over-estimated because iPP underwent reorganization during the DSC heating scan at a rate of 20°C/min. This reorganization was strongly

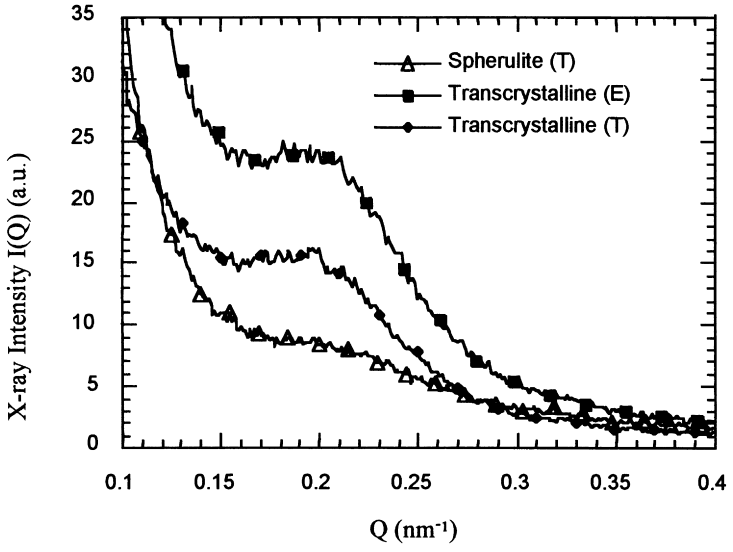

Fig. 11. SAXS intensity as a function of Q for all transcrystalline and all spherulitic iPP specimens with annealed condition. (T: through view, E: edge view.)

Table 3
Crystallinity, long-period and thermal expansion coefficient of iPP specimens with different birefringence

Birefringence	Crystallinity (DSC) (%)	Crystallinity (WAXS) (%)	Long-period (SAXS) (nm)	α [a]
Mixed	54	46	26	120
Positive	53	38	22	98
Annealed	53	52	33	100
Negative	59	50	30	101

[a] Thermal expansion coefficient (10^{-6} cm/cm/°C).

dependent on the initial crystallinity, and was not visible in the DSC thermogram. The specimens with positive birefringence had the lowest value for both the long period and crystallinity. Most crystals were formed in regime III with a much lower T_m^2, and the reorganization was expected to be more evident.

The melting behavior and the degree of crystallinity determined by DSC for all spherulite iPP with different birefringence are in good agreement with all transcrystalline iPP specimens, except for giving lower crystallinities for all spherulites determined by WAXS. The scaled amorphous curve may be over estimated in the WAXS method for all spherulite specimens.

Thermal expansion coefficients (α) are given in the fifth column of Table 3. Specimens with positive birefringence show the lowest thermal expansion coefficient (98×10^{-6} cm/cm/°C) irrespective of the lowest crystallinity. It may be due to the predominantly cross-hatched lamellae which hinder the thermal expansion of radial lamellae. The α value was 120 for the specimen with mixed birefringence. The α values are 100 and 101, respectively, for the annealed and negative ones due to the high crystallinities which were formed in regime II.

3.5. Interfacial shear strength of iPP/Kevlar fiber microcomposites

The interfacial shear strength of specimens is plotted versus birefringence in Fig. 13. Each bar represents an average of at least six tests. The error bar is also plotted along each data bar. The results indicate that the interfacial shear strength of iPP/Kevlar fiber composites changed significantly with birefringence. Specimens annealed at 160°C gave the best strength of 5.5 MPa while positive birefringence specimens exhibited a very poor adhesion with a value of 1 MPa. The results presented here (1–5.5 MPa) fit well with the interfacial shear strength values (4–5 MPa) published in the literature for iPP model composites which were tested by using the modified single fiber pull-out technique [5–7]. The highest average interfacial shear strength was only 16% of the tensile strength of pure iPP resin. Interfacial strength of specimens with mixed and negative birefringence was 1.8 and 3.3 MPa, respectively. The bonding between Kevlar 49 fiber and iPP is very poor because of the edge-on lamellae orientation [30].

Fig. 14 shows the PLM micrograph of the annealed specimens after the pull-out test. A poor adhesive type interfacial failure without any recognizable damage of the matrix was observed under PLM. When the fiber was pulled through a long fracture path, the Kevlar fiber embedded in the matrix gradually became somber. Before pulling through the matrix, small bright spots were seen on the fiber surface, whereas fiber fibrillation was formed when the Kevlar fiber was pulled out of the matrix. It is well known that Kevlar fiber has poor abrasion resistance because of its weak lateral bond forces [31]. Kevlar fiber fibrillates easily when it is rubbed against another matter and this fibrillation can be viewed as a process of splitting and fracturing of the fibrillar

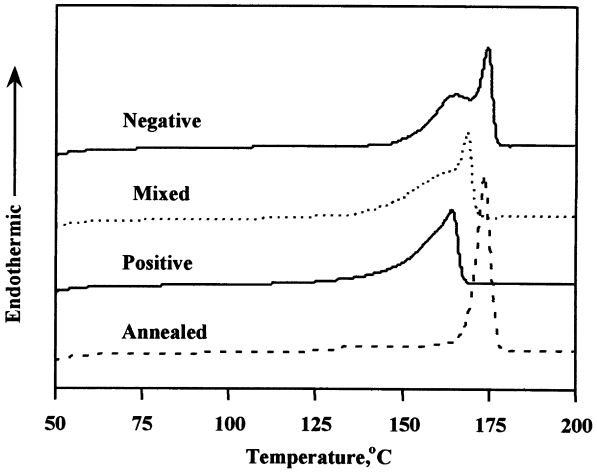

Fig. 12. DSC melting traces of all transcrystalline iPP specimens with different birefringence. The heating rate was 20°C/min.

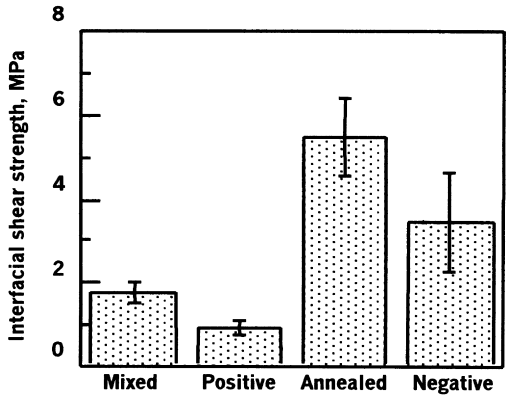

Fig. 13. Interfacial shear strength of iPP/Kevlar single-fiber microcomposites with different birefringence.

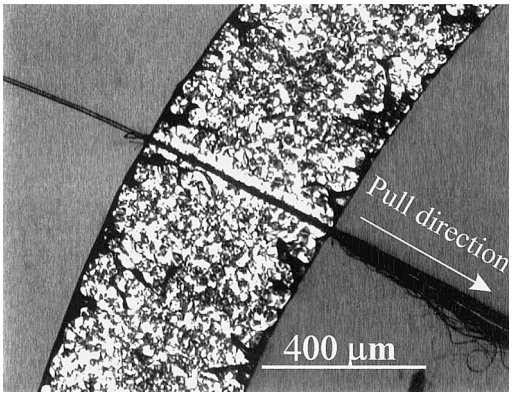

Fig. 14. PLM micrograph shows the fibrillation of Kevlar fiber during the single-fiber pull-out test. The scale bar corresponds to 400 μm.

structure in the fiber surface region. This fact indicates that the mechanical friction is a relevant factor for the interfacial adhesion in Kevlar/iPP system.

The experimental results reveal that samples with higher crystallinity have a better interfacial shear strength. It indicates that crystallinity plays an important role in the iPP/Kevlar fiber composites, which have the similar thicknesses of transcrystalline layer. This improvement could be related to thermal shrinkage in the interphase during crystallization and which resulted in higher contraction force. This contraction force is believed to give a great contribution on the mechanical interlocking [32], which originates from dispersive forces down to atomic scale. The crystallinity (determined by WAXS) of annealed and mixed birefringence specimens are 37 and 21% higher than that of positive birefringence specimens. However, the interfacial strength was 450 and 180% higher, respectively. One of the reasons is related to the thermal expansion coefficient. It is believed that the dominantly cross-hatched lamellae in positive birefringence specimens prevented the thermal expansion of the radical lamellae and led to a smaller value of the thermal expansion coefficient, which in turn decreased the thermal mismatch and decreased the shear strength. This is in consistent with the work of Dryden [33], who modeled the hydrostatic pressure in the center of the spherulite. It appears that if the radial stiffness of the spherulite is larger than its tangential stiffness, a compression will occur, while hydrostatic tension will be present in the opposite case.

Surface roughness has widely reported as a dominant factor in determining the transcrystallization [13]. It is recently stated that the initial nuclei might locate in the grooves of the substrate surface and become the anchored molecules that enhance the adhesion of fiber/matrix through mechanical interlocking [32]. That means that the effective mechanical interlocking is caused only by the radial lamellae, since the edge-on lamellae orientation is found in the iPP/Kevlar system [30]. The postulate is in agreement with those results obtained in this study. The birefringence (fraction of radial lamellae) in the interphase significantly affected the interfacial shear strength of iPP/Kevlar fiber composites. Higher radial lamellae fraction showed higher interfacial shear strength, whereas positive birefringence specimens, which have the most tangential lamellae, displayed very poor interfacial adhesion. It can thus be concluded that the more radial lamellae increase the radial stiffness relative to the tangential one, and produce higher normal stresses on the fiber surface. The stiffness enhancement within the transcrystalline layer caused by the higher crystallinity and radial lamellae fraction could be the major reason causing the improvement of the normal compression stress. That is, the birefringence of the transcrystalline interphase (the fraction of two lamellae compositions) significantly affected the interfacial shear strength.

Comparing the interfacial shear strength at the same thermal expansion coefficient and crystallinity, the strength obtained for annealed samples was higher than for specimens with negative birefringence and without transcrystalline layers. Crystallization induces a kind of noncrystalliable impurity expulsion which can thus create a weak impurity boundary [34,35] at the fiber/matrix interface when the fiber is covered with spherulites only. In connection with above discussion and the failure mode results, a failure mechanism was thus proposed to proceed through deformation processes involving the sliding of the edge-on lamellae and the detachment of the anchored molecules from the fiber surface.

4. Conclusion

The micromorphologic observation and supermolecular structure study presented here show that the optical birefringence change of iPP is related to the contribution of cross-hatch lamellae. The interfacial shear strength in the iPP/Kevlar fiber composite is significantly influenced by the crystallinity and matrix birefringence. Specimens with positive birefringence (or dominantly cross-hatched lamellae) hinder the thermal expansion of radial lamellae and decrease the interfacial strength. Fibrillation of the Kevlar fiber indicates that mechanical friction is a relevant factor for the interfacial strength. The more radial lamellae increase the radial stiffness relative to the tangential one, and produce higher normal stresses on the fiber surface. This stiffness enhancement within the transcrystalline layer caused by the higher crystallinity and radial lamella's fraction could be the major reason which improves the normal compression stress. It is therefore concluded that the optical birefringence in the transcrystalline layer significantly affected the interfacial shear strength, which was related to the mechanical friction, thermal mismatch, and the crystallinity.

Acknowledgements

Dr C.-M. Wu is thankful for the DAAD fellowship at the IVW in Kaiserslautern. The authors also wish to thank Prof.

S.-J. Bai for helpful discussion of SAXS experiments. This work was financially supported by the National Science Council, Republic of China, (NSC 88-2216-E110-019) and by the European Union through a BRITE Thematic Network project (BRRT-CT97-5004), respectively.

References

[1] Nagae S, Otsuka Y, Nishida M, Shimizu T, Takeda T, Yumitori S. J Mater Sci Lett 1995;14:1234.
[2] Felix JM, Gatenholm P. J Mater Sci 1994;29:3043.
[3] Yue CY, Cheung WL. J Mater Sci 1992;27:3181.
[4] Folkes MJ, Wong WK. Polymer 1987;28:1309.
[5] Kobayashi H, Hakayawa E, Kikutani T, Takaku A. Adv Compos Mater 1991;1:155.
[6] Hoecker F, Karger-Kocsis J. Polym Bull 1993;31:707.
[7] Moon CK. J Appl Polym Sci 1994;54:73.
[8] Wang C, Hwang LM. J Polym Sci Part B: Polym Phys 1996;34:1435.
[9] Ye L, Scheuring T, Friedrich K. J Mater Sci 1995;30:4761.
[10] Incardona S, Migliaresi C, Wagner HD, Gilbert AH, Marom G. Compos Sci Technol 1993;47:43.
[11] Klein N, Marom G. Composites 1994;25:706.
[12] Folkes MJ, Hardwick ST. J Mater Sci Lett 1987;6:656.
[13] Hata T, Ohsaka K, Yamada T, Nakamae K, Shibata N, Matsumoto T. J Adhes 1994;45:125.
[14] Klein N, Marom G, Pegoretti A, Migliaresi C. Composites 1995;26:707.
[15] Zeng H, Zhang Z, Zhang M, Xu J, Jian N, Mai K. J Appl Polym Sci 1994;54:541.
[16] Norton DR, Keller A. Polymer 1985;26:704.
[17] Cheng SZD, Janimak JJ, Zhang A. Polymer 1991;32:648.
[18] Bassett DC, Olley RH. Polymer 1984;25:935.
[19] Wu CM, Chen M, Karger-Kocsis J. Polymer (in press).
[20] Wu CM, Chen M, Karger-Kocsis J. Polymer 1999;42:4195.
[21] Olley RH, Bassett DC. Polymer 1982;23:1707.
[22] Wang C, Hwang LM. J Polym Sci Part B: Polym Phys 1996;34:47.
[23] Varga J. In: Karger-Kocsis J, editor. Polypropylene structure, blends and composites I: structure and morphology, London: Chapman and Hall, 1995 (chap. 3).
[24] Varga J. J Mater Sci 1992;27:2557.
[25] Binsbergen FL, De Lange BGM. Polymer 1968;9:23.
[26] Haudin JM. In: Meeten GH, editor. Optical properties of polymers, London: Elsevier, 1986 (chap. 4).
[27] Lovinger AJ. J Polym Sci: Polym Phys Ed 1983;21:97.
[28] Yeh CF, Su AC, Chen M, Sugimoto R. J Polym Res 1995;2:139.
[29] Ho HL, Mu CC. X-ray diffraction technique. Bejing: Textile Industry Publisher, 1988.
[30] Dean DM, Register RA, Rebenfeld L, Hsiao BS. Polym Prep 1997;38(2):48.
[31] Yang HH. Kevlar Aramid fiber. Chichester: Wiley, 1993.
[32] Wang C, Liu CR. J Polym Sci Part B: Polym Phys 1998;36:1361.
[33] Dryden JR. J Mater Sci Lett 1987;6:1129.
[34] Lee Y, Porter RS. Polym Engng Sci 1986;26:633.
[35] Hull D. Mater Sci Engng 1994;A184:173.